**Pergamon**

PII : S0017–9310(96)00296–7

# Some critical transitions in pool flash evaporation

JONG-IL KIM

Department of Mechanical Engineering, Chosun University, 375 Seosok-dong, Kwangju,
Republic of Korea

and

NOAM LIOR†

Department of Mechanical Engineering and Applied Mechanics, University of Pennsylvania,
Philadelphia, PA 19104-6315, U.S.A.

**Abstract**—To improve the fundamental understanding of the physics of the flash evaporation process, pool flash evaporation experiments were conducted in a 152 mm diameter chamber with initial water temperatures of 40–80°C, and superheats of 2–7°C. Several critical transition points were identified or discovered : (1) a critical time at which the rate of ebullition and evaporation diminishes abruptly, (2) an initial water temperature ($T_i$) at which the non-equilibrium temperature difference attains a minimum, (3) a critical initial water temperature at which the expected observed trend of decreasing non-equilibrium temperature difference (NETD) with decreasing depth reverses itself and (4) a critical initial pool depth at which $\partial^2(\text{NETD})\partial T_i^2$ changes sign from positive at smaller depths to negative at larger depths. © 1997 Elsevier Science Ltd. All rights reserved.

## 1. INTRODUCTION

Flash evaporation is used extensively in distillation and steam generation processes, including water desalination, thermal storage steam accumulators/generators, and ocean–thermal energy conversion. It is also of great importance in a wide variety of other applications, ranging from loss-of-coolant accidents in nuclear reactors to thin film coating under high vacuum. The flash evaporation phenomenon is typically very rapid and associated with violent disruption of the evaporating liquid, and is hence somewhat difficult to both model and measure.

Flash evaporation studies in pools of degassed distilled water were carried out by Miyatake *et al.* [1, 2] in a cylindrical vertical vessel of 80 mm diameter, at water depths of 100 mm and 200 mm, at initial temperatures of 40, 60, and 80°C, and superheats of 2.5–5.5°C, and by Gopalakrishna *et al.* [3] using both degassed fresh water and a degassed 3.5% (by weight) aqueous NaCl solution in a similar vessel but of 152 mm diameter, at water depths of 165, 305 and 457 mm, at initial temperatures from 25 to 80°C, and initial superheats of 0.5–10°C. In both experiments the flashing was initiated by rapidly exposing the water to a volume maintained at pressure lower than the

saturation pressure of the water corresponding to its initial temperature. As flash evaporation proceeded, the temperature of the water dropped gradually to an equilibrium value corresponding to the final pressure.

From their study, Miyatake *et al.* [1] found that flashing occurs in two consecutive stages : the initial very rapid, indicating vigorous ebullition, followed by relatively quiescent evaporation. They proposed correlations using dimensional parameters to predict the rate of evaporation and the non-equilibrium fraction NEF

$$\text{NEF} \equiv \frac{T(t) - T_e}{T_i - T_e} \qquad (1)$$

where $T_i$ is the initial bulk-average temperature of the water, prior to flashing, $T(t)$ is the bulk-average temperature of the water at time $t$ after flashing commenced, and $T_e$ is the equilibrium temperature after flashing practically ceased, corresponding to the equilibrium saturation pressure at that time, in the experiments equal to the measured vapor temperature $T_v$.

Gopalakrishna *et al.* [3] identified by dimensional analysis the dimensionless parameters which control flash evaporation rates in pools, and using their experimental data employed these parameters in developing a dimensionless correlation for the flash evaporation rate. They proposed that these dimensionless parameters are the Jakob number, Prandtl number of the

---

† Author to whom correspondence should be addressed.

## NOMENCLATURE

$c_p$  specific heat of the flashing liquid [kJ kg$^{-1}$ °C$^{-1}$]

$h_{fg}$  latent heat of evaporation of the flashing liquid [kJ kg$^{-1}$]

$H$  depth of liquid in the flash chamber [mm]

$H_r$  dimensionless depth, $\equiv z/H$

$H_{cr}$  critical depth of liquid in the flash chamber, at which the sign of $\partial^2(\text{NETD})/\partial T_i^2$ changes [mm]

$Ja$  Jakob number, $\equiv c_p\Delta T_s/h_{fg}$

$N_b$  the total cumulative number of bubbles detected

$\overline{N_b}$  the average cumulative number of bubbles detected ( $= 386$ bubbles)

$\hat{N_b}$  cumulative number of detected bubbles ratio, $\equiv N_b/\overline{N_b}$

NEF  non-equilibrium fraction, $\equiv (T-T_e)/(T_i-T_e)$

NEF  non-equilibrium fraction at end of flashing, $\equiv (T^*-T_e)/(T_i-T_e)$

NETD  non-equilibrium temperature difference, $\equiv T^*-T_e$ [°C]

$r$  radial position in the flash chamber [m]

$R$  flash chamber radius [m]

$t$  time [s]

$t_{cr}$  critical time, at which the rate of flash evaporation is reduced abruptly [s]

$t^*$  time till practical end of flashing [s]

$T$  temperature of water [°C]

$T_e$  equilibrium temperature of water, as defined by the saturation state corresponding to the vapor pressure in the flash chamber [°C]

$T_i$  initial bulk-average temperature of water [°C]

$T_{i,cr}$  critical initial bulk-average temperature of water, at which the NETD becomes independent of depth ($H$) and superheat ($\Delta T_s$) [°C]

$T_{i,min}$  initial bulk-average temperature of water at which the minimal NETD is attained (only valid for $H < H_{cr}$) [°C]

$T_v$  mean temperature of vapor [°C]

$T^*$  bulk-average water temperature after flashing practically ceased [°C]

$z$  water depth coordinate measured from free surface [mm].

Greek symbols

$\Delta p_s$  initial apparent pressure superheat, $p_i-p_e$ [Pa]

$\Delta T_s$  initial apparent superheat, $\equiv T_i-T_e$ [°C].

liquid, dimensionless hydrostatic head ($\Delta p/H$, where $\Delta p$ is the pressure superheat and $H$ is the liquid depth), and the salt concentration. They found that the flash evaporation rates increase slightly with the Jakob number and $\Delta p/H$, and that they were about 5% lower than those presented by Miyatake et al. [1].

The general conclusion from these studies is that the non-equilibrium temperature difference, NETD, defined as

$$\text{NETD} \equiv T^*-T_e \qquad (2)$$

where $T^*$ is bulk-average water temperature after flashing ceased (usually measured in these experiments about 10 s after the process initiation, when no bubbling is evident any longer), diminishes when the initial temperature is increased and when the superheat $\Delta T_s$, defined as

$$\Delta T_s \equiv T_i-T_e \qquad (3)$$

is decreased. Its normalized equivalent, the non-equilibrium fraction NEF, diminishes when the initial temperature and the superheat are increased. These results are consistent with the theories of bubble nucleation and growth in homogeneous boiling, and surface evaporation: higher temperatures promote evaporation because of the increase in vapor pressure and decrease of surface tension, latent heat of evaporation, and viscosity, and the superheat is the measure of the driving force for bubble nucleation and growth and for surface evaporation. It is noteworthy that the understanding of bubble physics is critical in this study, and more detailed information can be found in refs. [4–7].

In their experimental investigation of flashing in a shallower pool, Miyatake et al. [2] had the intriguing observation that while flash evaporation in shallower pools results in a lower NETD for $T_i = 40$ and 60°C, as expected from the fact that the hydrostatic head inhibiting bubble nucleation and growth is diminished, the dependence has reversed itself at $T_i = 80$°C for $H = 100$ mm. At this temperature the NETD became *higher* than that for the deeper pool of $H = 200$ mm, a result which is not intuitively expectable. In the same study, Miyatake et al. [2] observed that large bubbles were rapidly formed near the flash-tank bottom for $H = 100$ mm at 80°C, which they speculated to have caused strong bulk mixing, resulting in the lowering of the water temperature and consequently of the driving force for evaporation. It was also observed that while the downward-penetration depth of the bubble generation region increased moderately with $T_i$, yielding more evap-

oration, the trend was reversed at $T_i = 80°C$ for $H = 100$ mm. The explanation is plausible, since indeed these lower water depths and higher temperatures have a proportionally lower tendency to suppress bubble nucleation and growth, thus allowing under these conditions the generation of large bubbles which diminish flash evaporation rates as explained above.

Yet another phenomenon supports the observed trend reversal. Following the initial rapid decrease in vapor pressure due to the sudden opening of the flash chamber vapor space to the lower pressure vacuum tank, vapor release would tend to increase the pressure in this closed system because of the large difference between the specific volumes of water and vapor. This pressure increase was found in [2] to be insignificantly small at the higher temperatures investigated, but was most significant for the lowest temperature and water level tested, reaching about 20% of the initial pressure difference available for flashing, and thus diminishing the driving force for flash evaporation to similar extent. The reason for this strong effect is obviously the low hydrostatic head and the high specific volume of the evolved vapor at the lower temperatures.

In other studies of flash evaporation in pools, Hooper and Abdelmessih [8] and Peterson et al. [9] studied flash evaporation during rapid depressurization of liquid pools, in relation to loss-of-coolant accidents which might occur in nuclear reactors. The studies were primarily experimental, the former using water and the latter Freon-11 as the flashing liquid, and they were conducted for larger superheats than those in refs. [1–3]. It was shown [8] that a simple equilibrium model for heat-transfer controlled bubble growth over-predicted the bubble growth rate, especially at high initial superheats, and that there was a slight delay, of a few ms, between the release of pressure on the liquid and the first occurrence of nucleation. It was also stated [9] that no bubbles were observed at very low superheats of Freon-11, but vigourous bubble formation occurred at higher superheats [8]. The mass generation rate under such flashing conditions was found to be 10–12 times the rates during surface evaporation alone. In an attempt to study evaporation from LNG tanks, Clegg and Papadakis [10] studied rates of evaporation accompanying timewise-linear depressurization of a pool of saturated Freon-11. For saturation pressures of 7.5–10.5 kPa they found that surface evaporation occurred for superheats of up to 1.5 K, and ebullition did not occur up to saturation pressures of 5.5 kPa and depressurization rates of 2.8 Pa s$^{-1}$.

It was also found in the above studies that bubbles in flash evaporation are typically nucleated in the bulk of the liquid, but some special surfaces, such as Teflon, were observed in [11] to be rather effective nucleation sites in flashing water.

This paper describes experimental studies of pool flash evaporation, which were aimed at advancing fundamental understanding of the approach to equilibrium as affected by processes of bubble nucleation, growth, translation and departure, and their tightly coupled interaction with the fluid mechanics of both phases. Transient temperature distributions in a flash chamber were measured to determine the progress to equilibrium, and the process was observed visually. Since bubble nucleation, growth and motion have a dominant role in flash evaporation, both through the evaporation process itself and though their vigorous fluid-mechanics effects, bubble presence frequencies were also measured in some of the experiments.

## 2. THE EXPERIMENTS

The experiments were conducted with distilled and deaerated water (replaced after each experiment) in an apparatus shown in Fig. 1, which is similar to that of Gopalakrishna and Lior [3]. Due to the technique used for counting bubbles, a small amount of salt (0.1 g l$^{-1}$) was added to the distilled water, but only in the experiments in which bubbles were counted and no temperature distributions were measured (this low salt concentration would have had no practical effects on the process in any case). The flash evaporation was observed in a cylindrical vertical Pyrex glass vessel (No. 1 in Fig. 1) of 152 mm internal diameter and 610 mm height, placed concentrically within a transparent acrylic cylinder of larger diameter. The space between the cylinders was evacuated to provide high thermal insulation of the test vessel and thus minimize the effects of heat loss on the examined flash evaporation phenomena. The test vessel was piped to a large tank (0.253 m$^3$, No. 6 in Fig. 1) through a solenoid valve. The initial temperature of the flashed water was regulated by means of a thermostatically-controlled bath (items 4, 12 and 22) and a circulation pump (item 5). The vacuum in the tank (item 6) was adjusted by means of the vacuum pump and controller (items 2 and 12, respectively), and associated valving, to the level corresponding to the desired flash-down pressure (or temperature) difference.

The pressure in the test vessel (flash chamber) and the vacuum tank was measured by U-tube manometers (item 7), and the pressure difference between the test vessel and the tank was measured by a differential pressure transducer (item 9). Dry-ice traps (item 11) were used to isolate the manometers and the vacuum pump, to prevent vapor build-up in these units.

The temperature distribution in the flash chamber was measured, as shown in Figs. 2 and 3(a) by two "combs", one having 30 Cu–Constantan, 0.127 mm dia. thermocouples, and the other having 30 disk thermistors, ground down to a diameter 1.3–1.5 mm. Closer spacing of the sensors is provided around the free surface where the temperature gradients are expected to be the highest. Duplicate temperature measuring combs were used because they compensated for each other's deficiencies; while the thermocouples have much better stability characteristics than thermistors, and were thus used as the primary
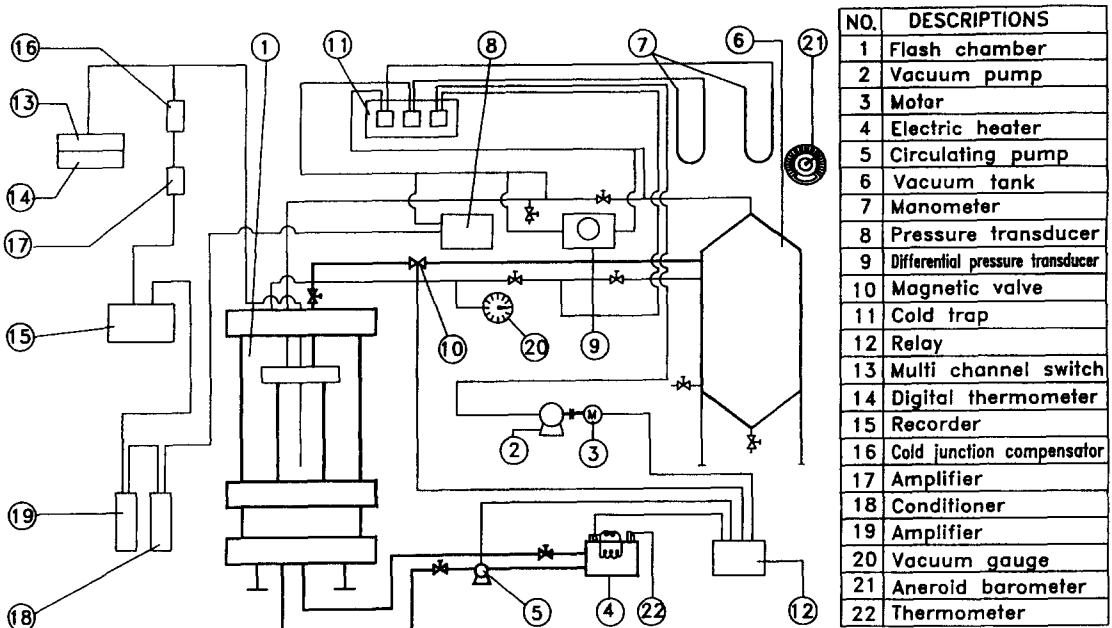
| NO. | DESCRIPTIONS |
|---|---|
| 1 | Flash chamber |
| 2 | Vacuum pump |
| 3 | Motor |
| 4 | Electric heater |
| 5 | Circulating pump |
| 6 | Vacuum tank |
| 7 | Manometer |
| 8 | Pressure transducer |
| 9 | Differential pressure transducer |
| 10 | Magnetic valve |
| 11 | Cold trap |
| 12 | Relay |
| 13 | Multi channel switch |
| 14 | Digital thermometer |
| 15 | Recorder |
| 16 | Cold junction compensator |
| 17 | Amplifier |
| 18 | Conditioner |
| 19 | Amplifier |
| 20 | Vacuum gauge |
| 21 | Aneroid barometer |
| 22 | Thermometer |

Fig. 1. Schematic diagram of the experimental apparatus.

temperature measuring sensor, their temperature sensitivity is orders of magnitude smaller. The thermistor comb was similar in principle to those described by Lior and co-workers [3, 12], but instead of the glass-encapsulated bead thermistors used in these references, economic reasons dictated the use of much less expensive (by about three orders of magnitude) and less stable disk-type thermistors in this study. To overcome the instability problem, the thermistors were calibrated immediately before the measurement, and used only once, primarily to examine the magnitude of temperature fluctuations.
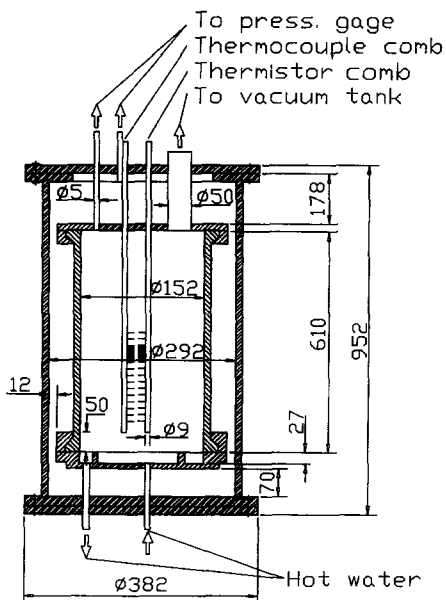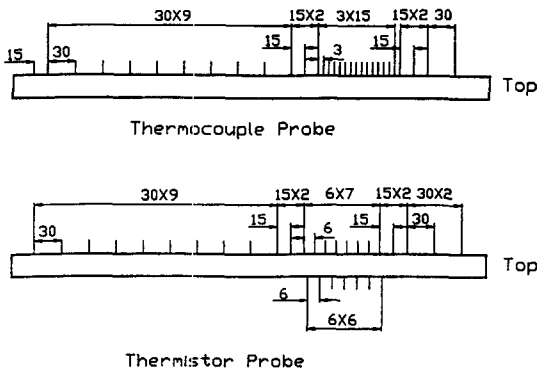


Fig. 2. The flash chamber (all dimensions in mm).

To measure distributions of the number of bubbles in the water, a probe capable of measuring the number of bubbles at 12 vertical and six radial locations simultaneously was constructed [Fig. 3(b)]. It is based on the electrical resistance principle [13–15], by which a high resistance pulse is recorded each time when a vapor bubble forms or passes between two small exposed electrode tips. The two electrodes of each local sensor were made here from 0.2 mm diameter enameled copper wires with an exposed tip, placed 0.127 mm apart, and an electric potential of 6 V d.c. was imposed between them. The number of bubbles passing at each of the sensors was determined by counting the number of pulses recorded by a multi-channel high frequency (500 Hz) photo-recorder over a measured time period. When used, this probe was placed in the flash chamber in lieu of the thermistor comb. The probe was found to detect 1.5% more bubbles than a Two-Phase Flow Signal Processor System Model 1109 designed to detect bubbles at a single location (made by Kagaku Kobyo Co., Japan).
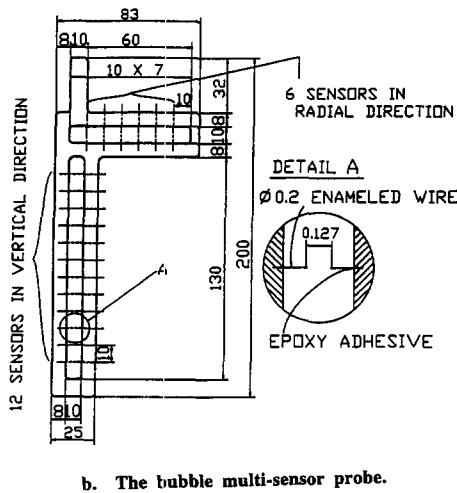
The stability and uniformity of the initial water temperature in the test vessel was within $\pm 0.1°C$. All the data were recorded by a multi-channel fast-response photo-recorder. The temperature measurement error was about $\pm 0.1°C$ and that of pressure was $\pm 0.5$ mm water column.

The experiments were conducted for initial water temperatures of 40–80°C at 10°C intervals, and for superheats of 2–7°C. The initial water level in the chamber was always 380 mm. Each experiment was repeated three to five times under the same conditions, to assure consistency and repeatability.

A stroboscopic photo setup with 1000 flashes $s^{-1}$ and a 1200 mm $s^{-1}$ streak camera, and a 60 fps movie

Thermocouple Probe



Thermistor Probe

**a. The temperature sensor combs.**



6 SENSORS IN RADIAL DIRECTION

DETAIL A
Ø0.2 ENAMELED WIRE

EPOXY ADHESIVE

**b. The bubble multi-sensor probe.**

Fig. 3. Instruments developed for the experiment (all dimensions in mm) : (a) the temperature sensor combs ; (b) the bubble multi-sensor probe.

camera were used to take pictures of the flashing phenomena, but the extremely rapid ebullition and mixing associated with the flashing prevented useful resolution for bubble growth examination.

## 3. RESULTS AND DISCUSSION

### 3.1. Temperature distributions

Figure 4 shows the transient vertical temperature distributions measured at the center of the vessel by the thermocouple comb for initial water depth of 380 mm. In general, the common feature of these distributions is that cooling of the water typically starts at the top (the free surface of the water) and with time propagates towards the bottom, phenomena which become more pronounced with the increase of superheat $(\Delta T_s)$ and initial temperature $(T_i)$. These observations are consistent with the fact that temperature reduction in the flashing water occurs due to evaporation, both from the free surface and from bubbles nucleated and growing in the bulk liquid. Not only

does surface evaporation promote cooling from the top, but also bubbles are more likely to nucleate and grow in regions of lower hydrostatic head, i.e. nearer to the free surface, and thus to be increasingly active in water cooling as the top is approached.

A number of the runs [cf. Figs. 4(b), 4(d), 4(e), 4(f), 4(h), 4(i), 4(k), 4(m) and 4(q)] show deviations from the behavior described above, in that the rate of cooling at the vessel bottom is comparable to that at the free surface or in some cases even exceeds it. This, we believe, is because the evaporation and heat transfer phenomena are not simply associated with just heat and mass diffusion, or even tranquil convection, but are strongly affected by the vigourous chaotic flow in the vessel arising from the rapid growth, agglomeration, and rise of bubbles. Such flows tend to strongly mix the evaporating liquid, counteracting any conduction-origined thermal stratification; furthermore, since bubble nucleation and agglomeration are of somewhat arbitrary nature, each run exhibits somewhat different transient behavior.

### 3.2. Flash evaporation rates

Faster flash evaporation rates bring the liquid closer to equilibrium sooner. The magnitude of the Non-Equilibrium Fraction NEF [defined by equation (1)] is plotted in Fig. 5(a) as a function of flashing time. Similar to the results in [1, 2], the first approximately three to four seconds of flashing are characterized by rapid rates of reduction of the NEF, after which time $(t_{cr})$ the rate of reduction of the NEF becomes significantly slower. Figure 5(b) shows the final NEF (NEF*) as a function of $\Delta T_s$ for $T_i = 54°C$ and $65°C$. The measured trends are consistent with the prior results described in Section 1 above: the non-equilibrium fraction decreases as the initial temperature and the superheat increase.

The measurement results of the cumulative number of bubbles ($N_b$, the total number of bubbles detected by all 12 bubble detection probes) shown in Fig. 6 support the measured trends of NEF and flash evaporation rates: an initial 3–4 s period of rapid increase in $N_b$, followed at the time $t_{or}$ by an abrupt transition to much more moderate rise in the number of bubbles during the remainder of flashing time, as well as a direct relationship between the magnitudes of $N_b$ and initial temperature and superheat. The rise of $N_b$ with NETD was also found to become steeper as $T_i$ increased.

Figure 7(a) shows that the cumulative number of bubbles measured by the horizontal (radial) part of the probe, placed just under the free surface, diminishes drastically in the radial direction, reaching near-zero values close to the flash chamber walls. This radial distribution was correlated by

$$\hat{N}_b(R_r) = 1.515(1 - R_r^2)^{1.2} \qquad (4)$$

where $\hat{N}_b$ is the cumulative number of bubbles ratio (defined in the Nomenclature), and $R_r \equiv r/R$, where $r$
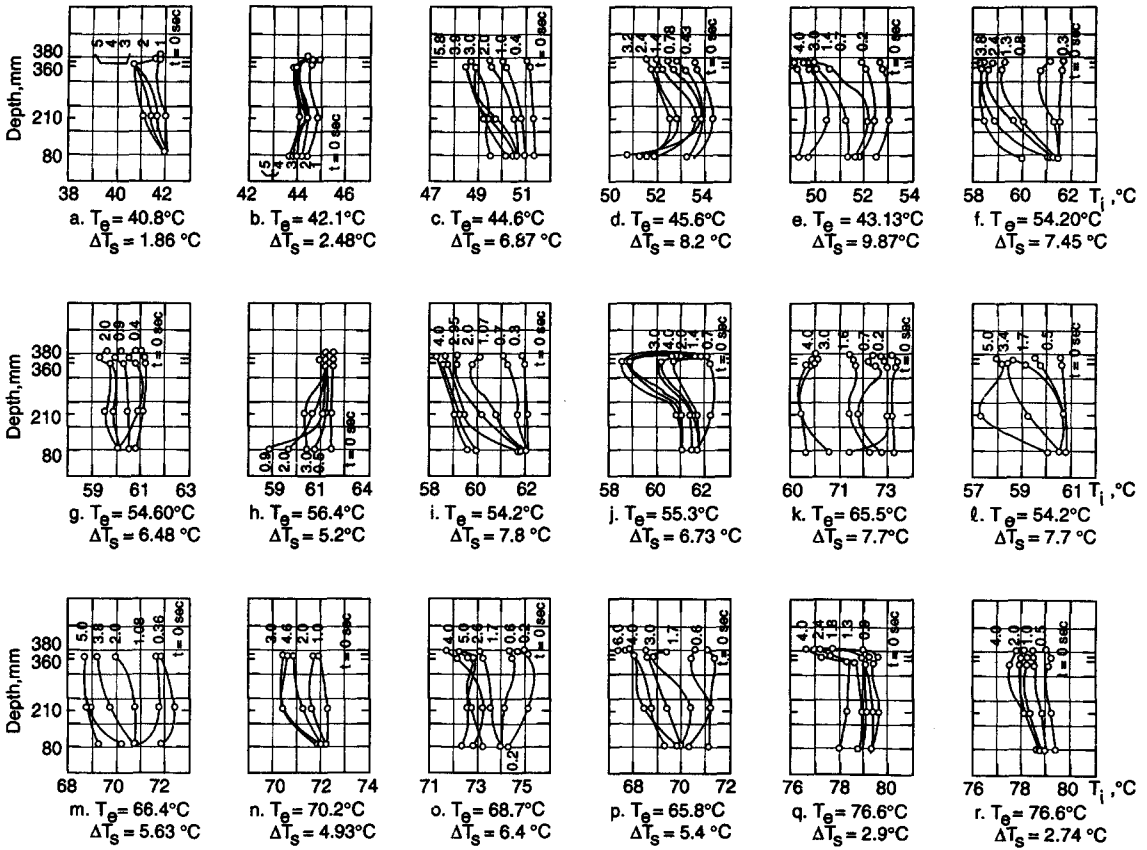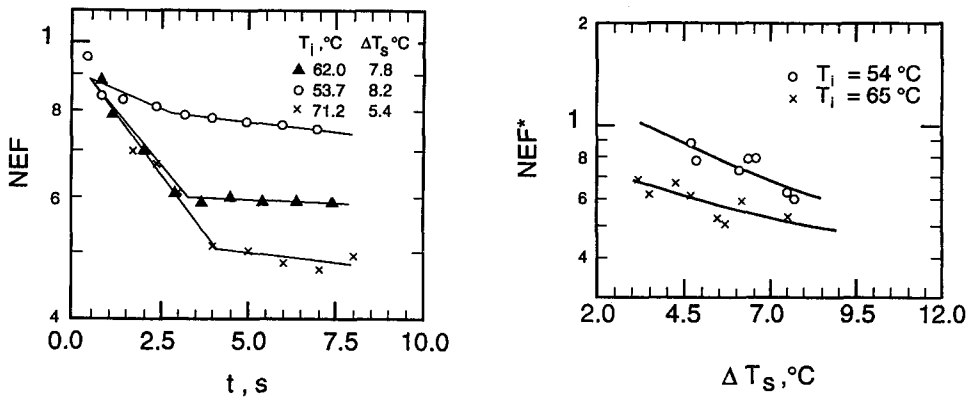
Fig. 4. The measured temperature distributions.



a. Non-Equilibrium Fraction (NEF) as a function of flashing time (t) for different initial temperature (T_i) and superheat (ΔT_s) combinations. Note: t_cr is the critical time at which the evaporation rate is abruptly reduced.

b. The final non-equilibrium fraction (NEF*) as a function of superheat (ΔT_s) for Ti = 54°C and 65°C.

Fig. 5. Equilibration results. (a) Non-Equilibrium Fraction (NEF) as a function of flashing time $(t)$ for different initial temperature $(T_i)$ and superheat $(\Delta T_s)$ combinations. Note: $t_{cr}$ is the critical time at which the evaporation rate is abruptly reduced. (b) The final non-equilibrium fraction (NEF*) as a function of superheat $(\Delta T_s)$ for $T_i = 54$ and 65°C.

is the radial position in the flash chamber and $R$ is its radius. As seen in Fig. 7(a), the correlation represents the trends well but has relative large errors near the wall. The rapid drop in the radial direction is probably

mainly due to hydrodynamic wall effects irrespective of any thermal influence, because the flash chamber was near-perfectly insulated.
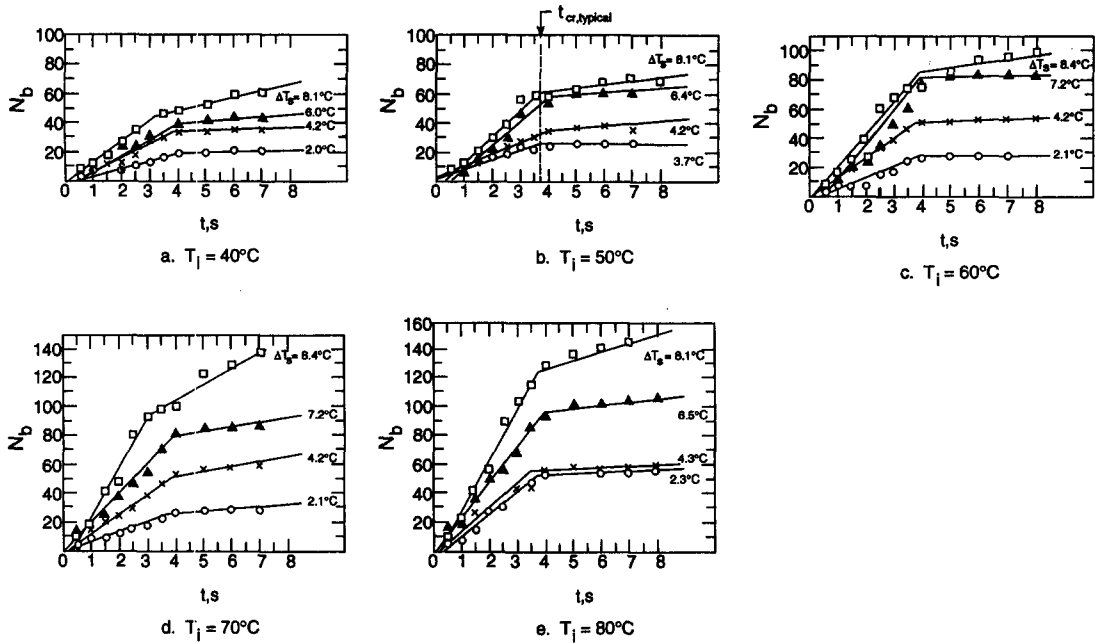
Figure 7(b) shows that the number of bubbles, as

Fig. 6. Cumulative number of bubbles ($N_b$) measurements as a function of flashing time ($t$) for different superheats ($\Delta T_s$). Note: $t_{cr}$ is the critical time at which the number of new bubbles and the evaporation rate are abruptly reduced.
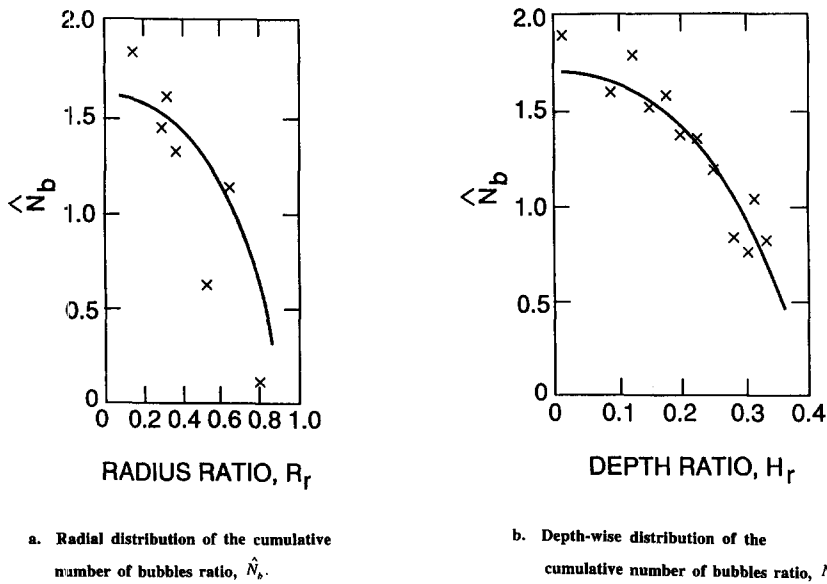


a. Radial distribution of the cumulative number of bubbles ratio, $\hat{N}_b$.

b. Depth-wise distribution of the cumulative number of bubbles ratio, $\hat{N}_b$.

Fig. 7. Bubble distributions in the water: (a) radial distribution of the cumulative number of bubbles ratio, $\hat{N}_b$; (b) depth-wise distribution of the cumulative number of bubbles ratio, $\hat{N}_b$.

measure along the chamber centerline by the vertical part of the probe, also diminishes with depth from the free surface. This is as expected due to hydrostatic head and inertia effects on bubble nucleation, growth, and rise, and the measured data were correlated with the depth ratio $H_r \equiv z/H$ by

$$\hat{N}_b(H_r) = 1.58(1 - H_r^2)^{8.5}. \tag{5}$$

The correlation represents the data with an error within about $\pm 5\%$.

### 3.3. Effects of water depth

Figure 8 shows the relationship between the measured non-equilibrium temperature difference (NETD) and the superheat ($\Delta T_s$) at different initial water temperatures ($T_i$), for water depth $H = 380$ mm, alongside with the results of Miyatake et al. [2] for $H = 100$ and 200 mm. From Fig. 8 for initial water temperatures of 40, 50, 60 and 70°C one can see that, as expected, NETD decreases with decreasing $H$ and with increasing $T_i$, and increases with $\Delta T_s$. It is also
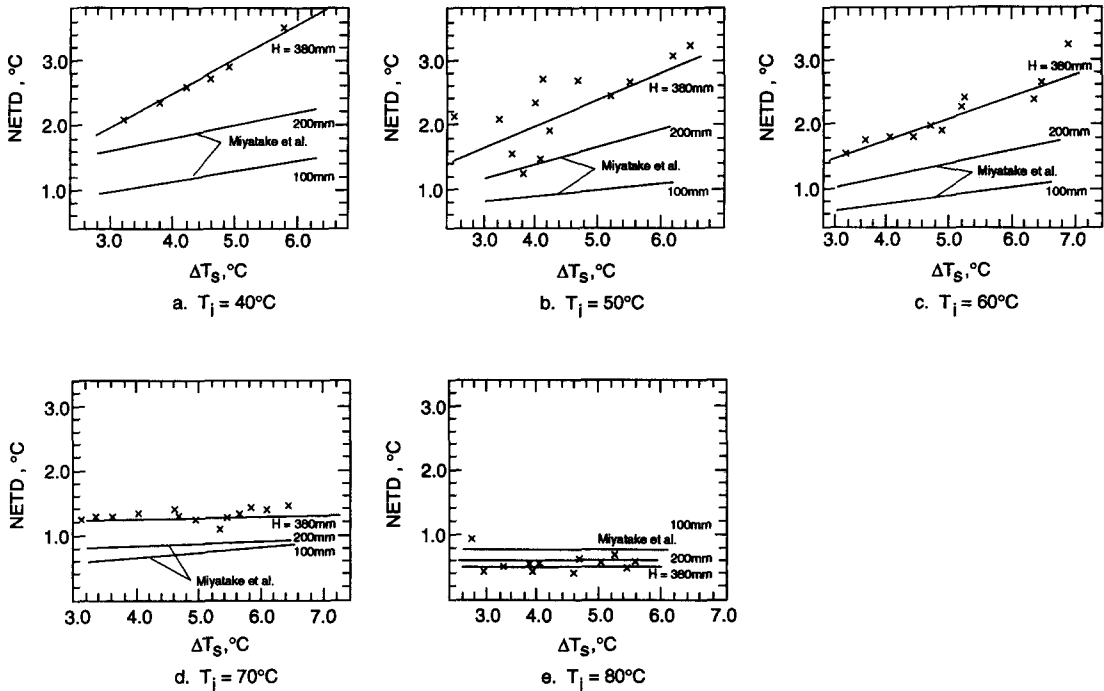
Fig. 8. Non-equilibrium temperature difference NETD as a function of the superheat ($\Delta T_s$) for different water depths ($H$). × 1, experimental data from this study.

seen that the effects of $H$ and $\Delta T_s$ diminish as $T_i$ is increased. As seen in Fig. 8(e), and in Fig. 9, our results for the deeper pool are consistent with those obtained by Myatake *et al.* [2] for shallower pools,



Fig. 9. Non-equilibrium temperature difference (NETD) as a function of initial temperature ($T_i$) for different superheats ($\Delta T_s$) and water depths ($H$). Note : $T_{i,cr}$ is the critical value of the initial temperature at which NETD is independent of $H$ and $\Delta T_s$.

showing a complete reversal of the effect of $H$ on NETD at $T_i = 80°C$ : the NETD is seen to increase with decreasing $H$.

Another interesting result from Fig. 9 is that $\partial^2(\text{NETD})/\partial T_i^2$ is positive for $H = 100$ mm, remains positive but seemingly smaller in magnitude when $H = 200$ mm, and becomes negative when $H = 380$ mm. A positive value indicates that the rate of decline of the NETD with $T_i$ diminishes as $T_i$ increases, implying that some equilibration (evaporation) retarding mechanism is becoming increasingly prominent. A negative value of this second derivative, on the other hand, indicates that the rate of decline of the NETD with $T_i$ is accelerated as $T_i$ increases, i.e. that equilibration is accelerated as $T_i$ increases. Generalizing these experimental results, the indication is that $\partial^2(\text{NETD})/\partial T_i^2$ is positive for small initial water depths, its magnitude decreases as depth is increased, and reverses its sign at some depth between 200 and 300 mm. In our experiments this critical depth, $H_{cr}$, at which this sign-reversal occurred was estimated to be between 246 and 295 mm. A plausible explanation of these observations lies in the interaction between the process of bubble generation and growth and the resulting fluid mechanics, as it occurs at different water depths and temperatures. Since, for a given temperature difference $T—T_e$, the pressure difference between vapor bubble interior and exterior rises strongly with $T_i$, the rate of bubble generation should also increase. At the same time, increasing rates of bubble generation and motion cause increased rates of mixing
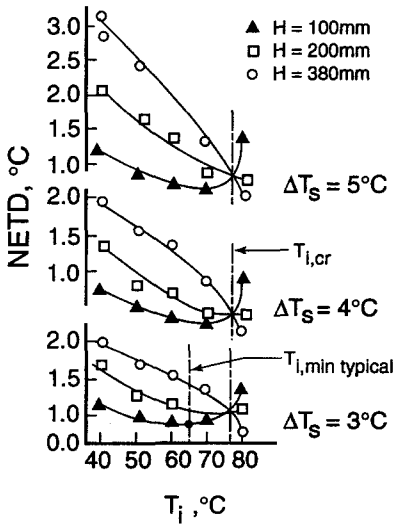
and thermal destratification of the water, thus lowering the temperature $T$ of the deeper water layers in which evaporation has not commenced yet. This reduces the driving force for bubble generation and growth, and thus tends to retard equilibration. Furthermore, the likelihood of bubble generation and growth in the chamber bottom region increases as the water depth, and thus the hydrostatic suppression head, are reduced. As observed by Miyatake et al. [2] and confirmed in our experiments, a relative large amount of bubbles is indeed formed near the chamber bottom for the shallower (around 100 mm and lower) water depths examined. As they rise, these bottom bubbles tend to roll the water over and thermally destratify it, leaving the bottom layer with a weak evaporative driving force and thus further from equilibrium. In deeper layers bubble formation is at first confined to the top layer, leaving the deeper water relatively undisturbed and at its original high temperature. With time, the flashing penetrates deeper and deeper into the water, until it reaches the bottom of the chamber. This allows closer approach to equilibrium of the entire volume of the water.

In summary, increasing $T_i$, with its accompanying increase in bubble generation rates, tends to equilibrate deeper layers much better than shallower ones, because the thermal driving force for evaporation in the latter is diminished due to bubble generation and motion and consequent mixing and destratification.

### 3.4. Effects of initial temperature

As seen in Figs. 8–9, increasing the initial temperature $T_i$ decreases, as expected, the NETD and its sensitivity to superheat and depth, for all temperatures, superheats and depths considered, with the exception of the above-discussed trend reversal for $H = 100$ mm which occurs at $T_i \approx 77°C$. At this temperature it is also seen that the NETD is independent of depth and superheat, identifying it as a critical transition temperature, to be denoted here as $T_{i,cr}$. This is further confirmed by the convergence of all of the NETD = NETD$(T_i)$ curves measured in this study for different superheats, to the point $T_i = 77°C$ = $T_{i,cr}$ where they intersect, as shown in Fig. 10.

More detailed examination of the shapes of the curves in Fig. 9 shows that the descending trend of the curves for $H = 100$ mm has actually reversed itself to an ascending one at a temperature lower than $T_{i,cr}$, having had minima (at a temperature $T_{i,min}$) which are slightly ascending with $\Delta T_s$: these minima are observed at $T_i = 68$, 71 and 72°C for $\Delta T_s = 3$, 4 and 5°C, respectively. While the curve for $H = 200$ mm does not have a minimum within the range of parameters displayed in Fig. 9, its shape indicates that a minimum might be reached at $T_i$ slightly higher than the 80°C upper limit of these experiments. Although, as discussed in Section 3.3 above, the shape of the curve for $H = 380$ mm does not indicate an approach to a minimum, physical reasoning points to the need for such a trend reversal at some higher values of $T_i$

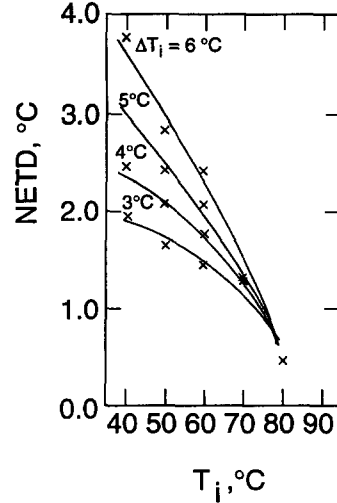

Fig. 10. Non-equilibrium temperature difference (NETD) a function of initial temperature $(T_i)$ for different superheats $(\Delta T_s)$ at water depth $H = 380$ mm. ×1, experimental data from this study.

even for this depth, because complete equilibration between the remaining liquid vapor is impossible within a finite time period.

### 3.5. Correlations of the non-equilibrium temperature difference

The following correlation was developed for the NETD measured in this study at $H = 380$ mm, when flash evaporation stopped,

$$\text{NETD}_{(H=380\,mm)}$$

$$= 0.6\Delta T_s \left[ 1 - \left( \frac{T_i - 48 - \Delta T_s}{40} \right)^2 \right]^{(0.5 + 0.1\Delta T_s)}. \quad (6)$$

Another correlation, for NETD$(H)$, was developed with depth $H$ as an additional independent variable, using all the experimental results of this study and of [2], thus valid for at least the depth range $100\ mm \leqslant H \leqslant 380\ mm$,

$$\text{NETD}(H) = (1.535\Delta T_s - 1.605)10^{-3} H + 0.5\Delta T_s$$

$$+ 0.2 + (0.0134 - 0.0122\Delta T_s)T_i$$

$$+ 10^{(\Delta T_s - 10)}(295 - H)\{\exp[(0.215 - 0.026\Delta T_s)T_i] - 1\} \quad (7)$$

where $H$ is in mm, and $T_i$, $\Delta T_s$ in °C. Both correlations, as seen in Fig. 9, represent the experimental data with an error within about $\pm 5\%$.

### 4. CONCLUSIONS

(1) Examination of the experimental data obtained in this study and elsewhere has revealed the existence of several critical transition points in pool flash evap-

oration: (a) a critical time, $t_{cr}$, of about 3–4 s in these experiments, at which the rate of ebullition and evaporation abruptly diminishes; (b) a minimal initial water temperature $T_{i,min}$ at which the non-equilibrium temperature difference NETD attains a minimum; (c) a critical initial water temperature $T_{i,cr}$ (here $T_{i,cr} = 77°C$), independent of $H$, at which the expected observed trend of decreasing NETD with decreasing $H$ reverses itself, yielding increasing values of NETD as $T_i$ increases above $T_{i,cr}$ and (d) a critical initial pool depth, $H_{cr}$, here between 246 mm and 295 mm, at which $\partial^2(NETD)/\partial T_i^2$ changes sign from positive at depths smaller than $H_{cr}$ to negative at larger depths. This is explained by the observation that for water depths smaller than $H_{cr}$ thermally-destratifying fluid mechanics effects tend to overcome the increase in bubble generation rates resulting from increasing $T_i$.

(2) Analysis of the measured temperature and bubble-count distributions, and of the approach to equilibrium re-emphasized the importance of the tightly-coupled interaction between bubble nucleation, growth and motion on the one hand, and of the associated fluid mechanics as exhibited by vigourous flows and mixing in the liquid on the other hand. This interaction governs the flash evaporation process, including the above-described critical transition points discovered in this study.

(3) A correlation for the non-equilibrium temperature difference, using the experimental data from this study and from [1, 2], was developed.

(4) A correlation was developed for the radial distribution of the number of bubbles. The number of bubbles drops off very rapidly as the flash chamber walls are approached. Since the chamber is near-perfectly insulated thermally, this implies that surrounding fluid mechanics effects, primarily due to bubble motion and growth, are dominant in bubble behavior during the flash evaporation process.

## REFERENCES

1. O. Miyatake, K. Murakami, Y. Kawata and T. Fujii, Fundamental experiments with flash evaporation, *Heat Transfer—Jap. Res.* **2**, 89–100 (1973).
2. O. Miyatake, T. Fujii, T. Tanaka and T. Nakaoka, Flash evaporation phenomena of pool water, *Heat Transfer—Jap. Res.* **6**, 13–24 (1977).
3. S. Gopalakrishna, V. Purushothaman and N. Lior, An experimental study of flash evaporation from liquid pools, *Desalination* **65**, 139–151 (1987).
4. A. Prosperetti, Bubble dynamics: a review and some recent results, *Appl. Sci. Res.* **38**, 145–164 (1982).
5. S. Gopalakrishna and N. Lior, Bubble growth in flash evaporation, *Proceedings of the 9th International Heat Transfer Conference*, Jerusalem, Israel, Vol. 3, pp. 73–78 (1990).
6. S. Gopalakrishna and N. Lior, Analysis of bubble translation during transient flash evaporation, *Int. J. Heat Mass Transfer* **35**, 1753–1761 (1992).
7. O. Miyatake, I. Tanaka and N. Lior, Bubble growth in superheated solutions with a non-volatile solute, *Chem. Engng. Sci.* **49**, 1301–1312 (1994).
8. F. C. Hooper and A. H. Abdelmessih, The flashing of liquids at higher superheats, *Proceedings of the 3rd International Heat Transfer Conference*, Chicago, U.S.A., Vol. 4, pp. 44–50 (1966).
9. R. J. Peterson, S. S. Grewal and M. M. El-Wakil, Investigations of liquid flashing and evaporation due to sudden depressurization, *Int. J. Heat Mass Transfer* **27**, 301–310 (1984).
10. G. T. Clegg and G. Papadakis, Rates of evaporation accompanying the depressurization of a pool of saturated Freon-11, *Chem. Engng Sci.* **41**, 3037–3043 (1986).
11. D. B. R. Kenning and K. Thirunavukkarasu, Bubble nucleation following a sudden pressure reduction in water, *Proceedings of the 4th International Heat Transfer Conference*, Paris/Versailles, France, Vol. 5, B2.9 (1970).
12. N. Lior, J. Leibovitz and A. D. K. Laird, A multiprobe miniature thermistor system of the measurement of temperature profiles, *Rev. Scient. Instrum.* **11**, 1340–1343 (1974).
13. ASME Heat Transfer Division, *Two-Phase Flow Instrumentation*. ASME, New York (1969).
14. Y. Iida and K. Kobayashi, An experimental investigation of the mechanism of pool boiling phenomena by a probe method, *Proceedings of the 4th International Heat Transfer Conference*, Paris/Versailles, France, Vol. 5, B1.3 (1970).
15. M. Sultan and R. L. Judd, Spatial distribution of active sites and bubble flux density, *Trans. ASME C* **100**, 56–62 (1978).